WiFED Mobile: WiFi Friendly Energy Delivery With Mobile Distributed Beamforming

Subhramoy Mohanti, *Graduate Student Member, IEEE*, Elif Bozkaya, *Graduate Student Member, IEEE*, M. Yousof Naderi, *Member, IEEE*, Berk Canberk, *Senior Member, IEEE*, Gokhan Secinti, *Member, IEEE*, and Kaushik R. Chowdhury, *Senior Member, IEEE*

***Abstract*— Wireless RF energy transfer for indoor sensors is an emerging paradigm ensuring continuous operation without battery limitations. However, high power radiation within ISM band interferes with packet reception for existing WiFi devices. The paper proposes the first effort in merging RF energy transfer within a standards compliant 802.11 protocol, realizing practical and WiFi-friendly Energy Delivery with Mobile Transmitters (WiFED Mobile). WiFED Mobile architecture is composed of a centralized controller coordinating the actions of multiple energy transmitters (ETs), and deployed sensors that periodically requires charging. The paper first describes 802.11 supported protocol features that can be exploited by sensors to request energy and for ETs to participate in energy transfer. Second, it devises a controller-driven bipartite matching algorithm, assigning appropriate number of ETs to sensors for efficient energy delivery. Thirdly, it detects outlier sensors (OS), which have limited power reception from static ETs and utilizes mobile ETs (METs) to satisfy their charging cycles. The proposed in-band and protocol supported coexistence in WiFED Mobile is validated via simulations and partly in a software defined radio testbed, showing that METs reduce latency by 42% and improve throughput by 83% in scenarios where using only static ETs fails to satisfy charging cycles of OS.**

***Index Terms*— Wireless energy transfer, distributed beamforming, software defined radio, resource allocation, quality of service.**

I. Introduction

THE pervasive deployment of heterogeneous sensors and small form-factor computing devices in homes and manufacturing floors is already showing tremendous gains in user-convenience, operational efficiency in terms of time and energy, and enhanced safety [1]. However, by design, these sensors are typically low-cost devices with limited energy storage capacity [2]. Contact-less wireless energy transfer is a promising technique that overcomes physical battery replacements and ensures continued, reliable operation. One such approach is based on focused RF radiation from energy-rich sources, which can then be stored at the sensors for future use [3], [4]. Specifically, through the method of distributed beamforming that involves synchronizing the carrier signal of individual transmitters, each transmitter signal can be made to combine coherently at the target receiver, achieving large gains [5], [6]. This synchronization approach scales to large numbers of transmitters, where each transmitter runs independent algorithms based on periodically transmitted feedback packets from the receiver. We achieve precise distributed beamforming through frequency locking enabled by an Extended Kalman Filter (EKF) that tracks the local oscillator offset between a transmitter and the receiver. EKF uses frequency offset measurements undertaken on the carrier signal of the feedback packet, while the phase adjustments for beamsteering are determined using a one-bit feedback that is provided by the receiver in the packet payload.

However, several challenges must be addressed to realize this vision of energy harvesting in sensors through distributed beamforming, specifically in terms of coexistence with other legacy wireless devices communicating in the ISM bands and the achievable energy yields to make the system practicable. Our previous work called WiFi Friendly Energy Delivery (WiFED) [7] addresses both these concerns by coexisting with and leveraging the 802.11 standard, as well as performing digital beamforming with the help of multiple different energy transmitters (ETs). However, it does not accommodate the scenarios when there is an insufficient number of fixed ETs, or sensors are situated at locations where they cannot receive enough power from the statically deployed ETs. In this paper, we enhance our previous approach by introducing mobile energy transmitters (MET) into the system architecture. WiFED Mobile not only schedules ETs to beamform energy to target sensors, it also orchestrates the path of METs to mitigate the impairment of overall energy and data performance originated from the sensors with low power reception.

WiFED Mobile operates in the presence of a regular 802.11 WiFi access point (AP) with its associated client stations (STAs). Our work is applicable to forward looking WiFi standards, including 802.11ac and beyond, which incorporates

Manuscript received April 29, 2020; revised December 11, 2020; accepted February 17, 2021; approved by IEEE/ACM TRANSACTIONS ON NETWORKING Editor G. Zussman. Date of publication March 2, 2021; date of current version June 16, 2021. This work was supported by the U.S. National Science Foundation under Grant CNS-1452628. *(Corresponding author: Subhramoy Mohanti.)*

Subhramoy Mohanti, M. Yousof Naderi, and Kaushik R. Chowdhury are with the Department of Electrical and Computer Engineering, Northeastern University, Boston, MA 02115 USA (e-mail: smohanti@coe.neu.edu; naderi@coe.neu.edu; krc@coe.neu.edu).

Elif Bozkaya is with the Department of Computer Engineering, National Defense University Naval Academy, 34942 İstanbul, Turkey (e-mail: ebozkaya@dho.edu.tr).

Berk Canberk and Gokhan Secinti are with the Department of Computer Engineering, Istanbul Technical University, 34469 İstanbul, Turkey (e-mail: canberk@itu.edu.tr; secinti@itu.edu.tr).

Digital Object Identifier 10.1109/TNET.2021.3061082

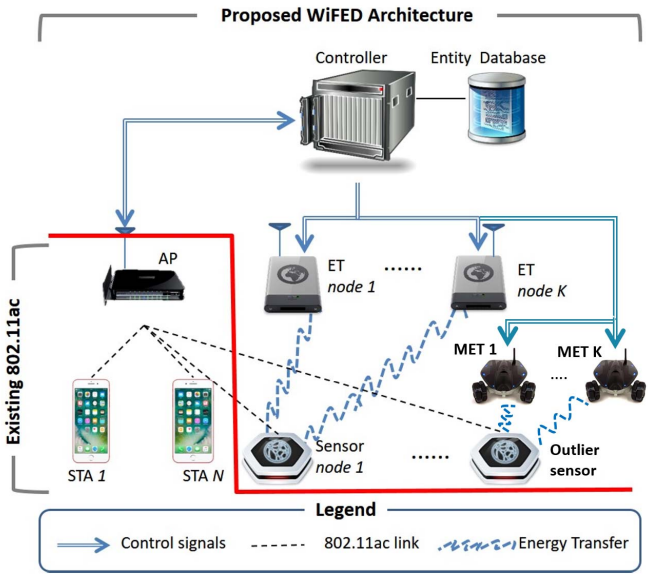

Fig. 1. WiFED Mobile architecture for energy delivery with distributed beamforming over existing 802.11ac network.

advanced features at the MAC layer that we will describe later in the paper. For concrete implementation example and without loss of generality, we shall directly reference 802.11ac standard in the subsequent discussion. WiFED Mobile components are given in Figure 1: (1) deployed IoT sensors that have a compatible 802.11ac WiFi radio and interfaced with an RF harvesting circuit; (2) multiple distributed ETs, each consisting of a radio with two operational modes: one that supports 802.11ac and the second mode that transmits an unmodulated continuous wave signal with maximum possible power ($\leq 3W$ as per FCC rules) [8]; (3) a controller that coordinates the energy transfer process, which can either exist as a separate device or be embedded as a software entity within the AP; and (4) it detects outlier sensors (OS) that threaten the overall system performance due to their limited or non-existent power reception and coordinates METs to manipulate physical plane in order to sustain charging cycles without disrupting data communication.

A. WiFED Mobile Motivation and Novelty

Existing 802.11-family of protocols are not designed for coexistence with heterogeneous networks. Moreover, 802.11 based distributed co-ordination function (DCF) poses unfairness problems between uplink and downlink flows [9]. Thus, even if highly efficient RF energy transfer is achieved, it is difficult to implement this in practical co-channel home/factory environments. Several IoT applications may provide critical services that require the sensor to be always operational. In such cases, the energy transfer takes priority. WiFED Mobile leverages existing 802.11ac protocol features to provide this differentiated channel access priority between energy and data transfers. Solutions such as a specialized MAC [10], [11] or modulating the energy signal with data [12] require changing existing WiFi infrastructure and rely on non-standardized protocols. WiFED Mobile is designed ground-up to facilitate both compatibility and coexistence with the 802.11ac (and later) standards; it can be deployed with current off-the-shelf hardware. Finally, WiFED Mobile addresses a fundamental problem in indoor deployments of selecting an optimal subset of ETs for each incoming energy request from a target sensor.

B. Conceptual Overview of WiFED Mobile Operation

WiFED Mobile builds on top of the existing 802.11ac WiFi architecture by innovatively introducing an energy plane along with the existing data and control planes. Here, the 802.11ac compatible AP manages all STA nodes (sensors and other users) in its Basic Service Set (BSS). The energy requests originate from individual sensors and are transmitted in the form of regular data packets towards the centralized controller, via the AP. The controller keeps a database of all registered sensors and ETs. The controller now identifies the optimal subset of sensors and outlier sensors, via a bipartite matching algorithm, to create and assign groups of ETs to requesting sensors and to control the movement of METs. It then instructs the AP to set up a contention-free period (CFP) for the energy transmission as well as initializes the ETs for the upcoming energy transfer, specifying the duration for which the target sensors should be charged. The energy transfer duration is upper bounded to ensure that data communication occurs fairly within the same channel.

The rest of the paper is organized as follows: Sec. II describes the related works and Sec. III presents the preliminary experiments that justify and motivate the WiFED Mobile design. In Sec. IV, we explain the details of WiFED Mobile system operation. The WiFED Mobile energy scheduling framework is explained in detail in Section V. We perform extensive performance evaluation studies in Section VI. Finally, Section VII concludes the paper.

II. Related Work

In this section, we review the most relevant works in two areas as follows.

Wireless Charging Protocols and Platforms: Protocols and platforms for RF energy transfer and harvesting have been comprehensively surveyed recently in [1] and [13]. MAC protocols that investigate the impact of sensor placement, frequency of operation, and number of RF energy transmitters on wireless charging time for optimizing energy delivery while minimizing its effect on data communication have been proposed in [10], [11]. However, a clean-state MAC design is difficult to implement without costly integration overheads. Self-sustainable wireless nodes that harvest ambient RF energy in cognitive radio networks is proposed in [14]. Here, low power secondary nodes harvest energy from nearby high power primary nodes. However, realistic power levels for such an architecture are not possible for indoor scenarios, along with additional challenges associated with spectrum management. Other works include harvesting energy from the received signals using time switching and power splitting methods while minimizing the impact on data performance [15]. The work presented in [16] is closest to

our approach of wireless energy transfer, by using distributed beamforming. However, this proposed method requires a large number of energy transmitters, and precise positioning of the transmitters and receiver to realize a practical wireless energy transfer solution. The study in [17] proves the need for focused RF radiation based reliable and efficient energy transfer methods through experiments conducted on a real test bed. The authors in [18], use numerical analysis over different antenna assignment strategies for wireless energy transfer, but they do not consider any other information related to devices such as topological deployment, battery charge, although such information is crucial in practical deployment scenarios. All these works, while furthering the state-of-the-art, do not focus on WiFi coexistence, and require considerable engineering of the protocol stack. The problem of charging multiple devices by a limited set of energy transmitters is considered in [19]. WiFED Mobile also incorporates this approach but under realistic characteristics of RF energy harvesting circuits.

Energy Transfer and Data Co-existence: Co-channel data and energy transfer is proposed in [12] by introducing a novel physical layer modulation scheme where the sender introduces variations in the envelope of the energy signal to communicate data. This scheme requires complex synchronization with existing upper layers of network and available hardwares. [20] studies the effect of ET placement on the charging rate of the sensor nodes and impacts on data communication, quantitatively analyzing the tradeoffs between wireless energy harvesting and data transfer.

III. Experiments on Distributed Beamforming

In this section, we describe our preliminary experiments to evaluate the distributed beamforming, channel gain and co-existence mechanisms in order to benefit both energy and data transfer processes in the 2.4GHz ISM band. Specifically, we observe (a) relation between beamforming and channel gain and (b) interference and performance characteristics between 802.11ac data and energy transmission with (i) continuous energy beamforming, (ii) random energy beamforming, and (iii) WiFED Mobile framework.

• **Beamforming impact on channel gain with static nodes:** In our first set of experiments, our goal was to observe the relation between channel behavior and beamforming performance, with and without transmit beamforming with multiple antennas and understand if it was feasible to leverage the advantages of beamforming in distributed energy transfer. We perform a 'Proof-of-Concept' experiment with an existing transmit beamforming solution available in Matlab [21]. We used two Ettus® X310 radios, each with two UBX daughterboards and two omnidirectional antennas, performing the role of transmitters. An Ettus® B210 radio was used as the receiver, and placed 2m away from the transmitters. To synchronize the transmitter and receiver radios, we used an Ettus Octoclock to generate the 10MHz reference signal for frequency synchronization and pulse per second (PPS) for time synchronization of all the radios. In this Matlab based beamforming algorithm, based on the reception of the transmitted signals, the receiver radio was programmed to update the channel state information every 700ms, which is the duration of a single iteration of the algorithm. The transmitter radios use the channel state information as a reference to update their respective beamforming weights. After turning on the receiver radio, the channel gain was measured at the receiver, at each instance of increasing number of transmit beamforming antennas. Figure 2 shows that the capacity of the channel improves linearly with increase in the number of transmit antennas, through the increase in the channel gain. To compute the channel gain, we extract the channel state information (CSI) at each time instant at the receiver. The absolute value of this instantaneous channel state estimation gives us the instantaneous channel gain (linear) value. We plot this over an example time period, as shown in Figure 2. When multiple transmitters are beamforming to a specific receiver, then, due to the effect of phase and frequency synchronization, the transmitted signals have an effect of 'constructive addition' at the receiver. In this case, the received amplitude becomes the sum of amplitudes of the individual beamforming transmitters. The resulting channel gain at the receiver, calculated as the absolute value of the channel state estimate at the receiver, reflects the same trend. However, this 700ms processing delay may not be practical in real world scenarios. Thus, for our proposed distributed beamforming in WiFED, we use a faster GnuRadio based algorithm, which we describe in the next experiment. One important aspect to observe from Figure 2 is that the variation of the channel is very small in time for a given set of transmitting antennas, which reduces the error in channel estimation for beamforming. As a result of this improvement in channel estimation, the corresponding received power at the receiver also improves with increasing number of transmit antennas, given in Figure 3, the detailed explanation of that experiment being given next. These results served as the baseline performance metric for the beamforming algorithm when the nodes are static.

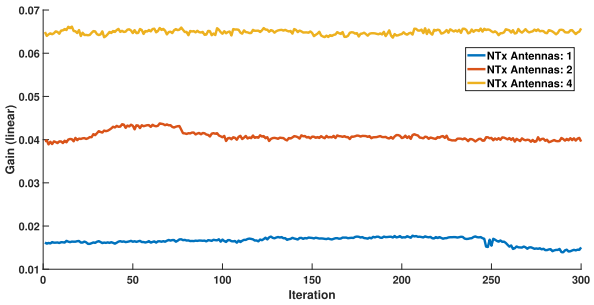

Fig. 2. Total channel gain using static nodes in indoor beamforming with different number of antennas.

• **Distributed Energy Beamforming Experiments**: In the next step, we demonstrate the feasibility of a distributed energy transfer network that uses beamforming through real testbed [5], [6], where multiple ETs are synchronized in phase and frequency in real time using periodic feedback from the target sensor, but without any common clock reference. This algorithm is faster than the earlier Matlab based beamforming approach, with the maximum processing delay at each transmit/receive nodes being around 50ms. Here, multiple ETs

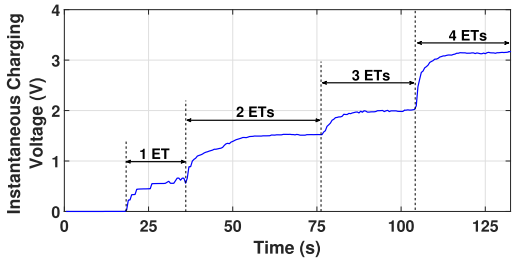

Fig. 3. Instantenous charging voltage at receiver with 1, 2, 3 and 4 ETs beamforming sequentially.

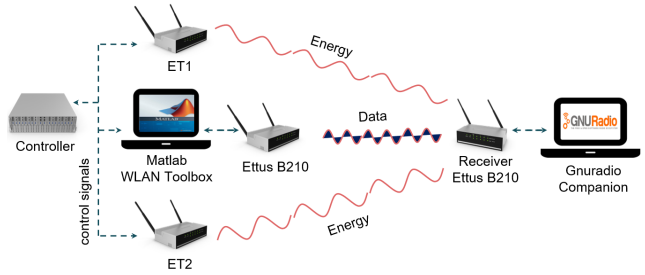

Fig. 4. Topology for 802.11ac and wireless energy transfer co-existence experiment setup.

are synchronized in phase and frequency in real time using periodic feedback from the target sensor, but without any common clock reference. The synchronization approach scales to large numbers of transmitters where each transmitter runs independent algorithms based on periodically transmitted feedback packets from the receiver. The frequency locking method employs an Extended Kalman Filter (EKF) to track the local oscillator offset between a transmitter and the receiver. The phase adjustments for beamsteering are determined using a one-bit feedback inserted into the feedback packet payload. The receiver broadcasts this one bit to indicate the change in its received signal strength in each feedback packet. Each transmitter uses this to make phase corrections (on top of the frequency/phase corrections for frequency locking based on the EKF) for beamsteering, using the randomized ascent algorithm first proposed in [22]. The convergence speed of the synchronization with this setup equals the sum of the time needed for frequency and phase locking. With a proper initial estimate for the LO frequency offset, the frequency synchronization can be brought down to as low as few ($<$10) cycles. Our empirical observation reveals that with three transmit nodes, the one-bit feedback algorithm typically converges in less than 20 cycles, corresponding to 1s in this setup.

Our beamforming setup consists of the following components 1) Four programmable ETs with omnidirectional antennas, 2) one RF-energy harvester circuit, and 3) controller software. A programmable ET is basically a Universal Software Radio Peripheral (USRP) connected to a power amplifier. The RF-energy harvester is fabricated and connected to a TI EZ430 sensor. The GNURadio software plane in the USRPs implements the beamforming algorithm for phase and frequency synchronizations, and transfers high power energy signals toward the desired receiver using a power amplifier with maximum allowable power. Using distributed energy beamforming, ETs self-adjust their in-phase based on feedback from the receiver, so that maximum net energy is transferred towards the intended receiver. The ETs organize themselves into a virtual antenna array and focus their transmission energy in the direction of the sensor, such that the emitted waveforms add up constructively at the target sensor. If all radios have the same antenna gain G_t and transmission powers P_t, with the receiver gain be G_r, then the received power P_t^r at the receiver node simplifies to:

$$P_T^r = P_t G_t G_r (\frac{\lambda}{4\pi})^2 \Big[\sum_{i=1}^{N} \frac{1}{R_i^2} + \sum_{i=1, i\neq j}^{N} \sum_{j=1}^{N} \frac{\cos(k\Delta R_{ij}))}{R_i R_j} \Big] \quad (1)$$

where $k = 2\pi/\lambda$ is the wave number of the energy wave (i.e., magnitude of the energy wave vector), $R_i = [(x_r - x_i)^2 + (y_r - y_i)^2]^{1/2}$ is the Euclidean distance from radio i to receiver and $\Delta R_{ij} = R(i) - R(j)$ is the difference between distances of radio i and j from the receiver. This analytical model for received power can be used to find the charging efficiency from N energy transmitting radios to each sensor [20]. In our first set of energy beamforming experiments, four ETs are placed 20cm away from each other in an array, each connected to two 50Ω omnidirectional antennas. The distance from the transmitters and receiver are fixed at 1m. The ETs are successively turned on to perform beamforming and with all ETs having equal transmit power of 3W, we measure the different levels of energy at the receiver. From Figure 3, we see that the harvested voltage at the receiver increases linearly with the increase in the number of ETs as the received power increases exponentially. The beamforming process organizes the ETs co-operatively into a virtual antenna array and focuses their transmission in the direction of the sensor. At the sensor-end, we also have the RF energy harvesting circuit for wireless charging of the sensor. The ETs make sure their transmission has a constructive interference effect at the sensor, which leads to a factor of N gain in power efficiency [20], where N is the number of collaborating ETs. Thus, if the power of each transmitter is fixed, then distributed beamforming results in N^2 gain in received signal-to-noise ratio (SNR). This arises from a factor of N gain due to increase in total transmit power, and a factor of N gain in power efficiency due to increased directivity from beamforming. Thus, our experiment validates the analysis in (1) and demonstrates the ability to efficiently transfer energy to sensors during their normal course of operations.

• **802.11ac and Energy Co-existence Experiments**: To characterize the effects of energy transmission in the ISM band of 2.4GHz during 802.11ac WiFi data communication, we create a 802.11ac WiFi AP and STA through Ettus USRP radios, and place two ETs 1.5m apart from the WiFi link, the setup of which we show in Figure 4. The 802.11ac OFDM VHT packets, generated by the MATLAB WLAN toolbox on the host machine, is transmitted using the connected USRP radio. On the receiver side, we use GNURadio companion to receive the data packets through the receiver USRP radio. For energy transfer, we use two other ETs tuned to the same 2.412 GHz with the host computer running the distributed

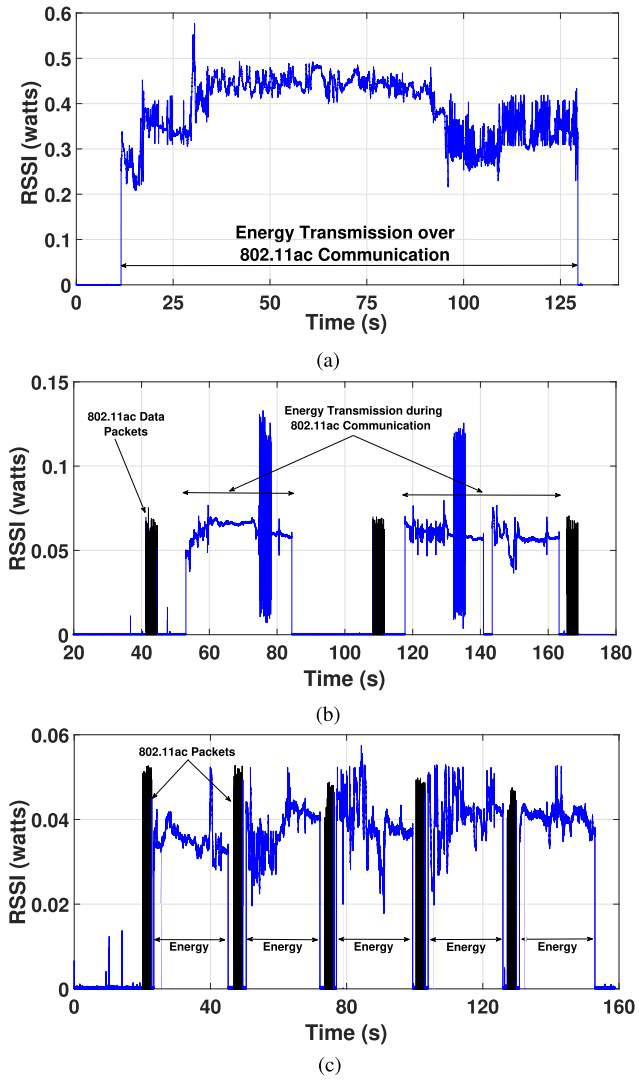

Fig. 5. Effect of energy transfer in different modes: (a) continuous energy transfer, (b) random energy transfer, (c) controlled energy transfer.

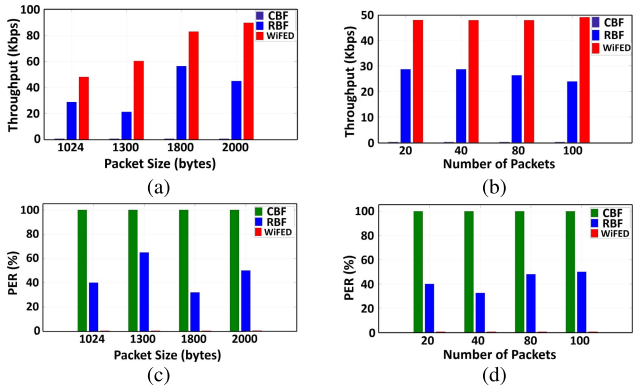

Fig. 6. Data performance characteristics of throughput with (a) changing packet size (b) number of packets. PER with (c) packet size and (d) number of packets in three modes of energy transfer.

beamforming algorithm. All of the host computers communicate with the controller via wired ethernet connections. The controller determines the duration and schedule of the energy beamforming to be either continuous, random or based on the WiFED framework. The WiFi transmission uses 1 space-time stream of QPSK rate 1/2 configured for 160MHz bandwidth with the controller accurately scheduling transmission in the final scenario. We conduct the experiment with varying packet sizes of 1024, 1300, 1800 and 2000 bytes, each time with 20 packets in a data slot and a total of 5 data slots.

• **Observations** We present our observations on concurrent energy and data transfer from the three modes of energy transfer through Figures 5 and 6 respectively. In Figure 5(a), we see that receiver only gets the energy signals at 0.4 Watts through continuous energy beamforming, while the data transmission gets completely interrupted by the higher power energy signal. As shown in Figure 6, throughput is negligible with 100% packet error rate (PER). In Figure 5(b), we observe the effects of signal reception when energy is transmitted at random intervals irrespective of data transmission. In this scenario, there is a high probability of data signals being interrupted by a random energy transfer. Though this is an improvement over the previous scenario of continuous energy transfer, this too adversely affects the data communication. As we can see from Figure 6, random interfering energy signal causes the WiFi receiver to attain almost half of the best achievable throughput with around 40% PER. We compare these measurements with synchronized signal transmission scheduling shown in Figure 5(c). Here, we observe the controller synchronizes the energy transfer in between concurrent data transmission slots to avoid interference and enables co-existence with WiFi. We see that the throughput in Figure 6 achieves near-optimal rates in the absence of any interfering non-cooperating protocol, with negligible PER. Thus, we adopt this controller-driven synchronized approach in WiFED Mobile where the data communication is silenced through channel reservation using standards-defined 802.11ac protocol features.

IV. WiFED Mobile With 802.11ac-Based Channel Access

WiFED Mobile operates the sensors in the Transmission Opportunity Power Save mode (TXOP PSM), as defined by the 802.11ac standard [23]. In this mode, the radio is kept switched off as a default case (called as Doze state), with periodic wakeup to check for currently buffered packets at the AP or to transmit new packets to the AP.

A. Managing Sleep-Cycles Through 802.11ac

The pending packets at the AP for the sensors are informed via the Traffic Indication Map (TIM), transmitted in every beacon interval. Sensors wake up in the beacon transmission intervals to monitor downstream traffic. During a data transmission, sensors not involved in the ongoing transmission or reception consume a significant amount of energy in overhearing. To overcome this problem, TXOP PSM allows the sensor to sleep whenever it listens to a TXOP, in which the AP sends data to another STA. To do so, the AP indicates the duration of the ongoing TXOP in transmitted frames. Whenever a user receives a frame destined for another STA, a given sensor can

TABLE I
ENERGY LEVEL CLASSIFICATION

$UnusedFieldBits$	$EnergyRange(volts)$
00	1.8 - 2.25
01	2.26 - 2.7
10	2.71 - 3.15
11	3.16 - 3.6

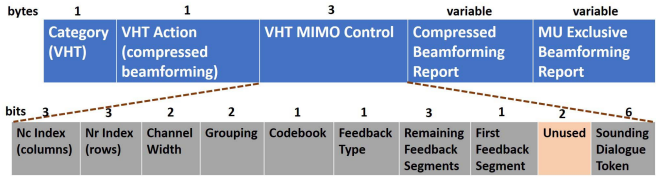

Fig. 7. WiFED Mobile insertion of bit level sensor energy information in 802.11ac compressed beamforming action frame.

switch to the sleep state and return to the awake state at the end of the TXOP. This operation, referred to as microsleep, lets the sensor sleep during short periods of time in which the channel is busy (typically, some tens, hundreds, or thousands of microseconds) [23].

B. Transmitting Energy Requests

Next, we describe how a sensor conveys its residual energy level to the controller through existing protocol fields defined by the 802.11ac standard. Specifically, we use the channel sounding function shown in Figure 8, which is periodically executed every 10ms-100ms by the AP, depending upon whether it is performing single-user or multi-user beamforming [24]. To achieve this, the AP sends out a Null Data Packet (NDP) after each NDP Announcement (NDPA) frame. Upon receiving the NDP, each associated STA in the network, including the sensors, reply back with the channel information in the Compressed Beamforming Action (CBA) frame. To query specific users, AP sends out the Beamforming Report Poll (BRP) for channel sounding measurement feedback following the NDP frame [25]. While the CBA frame is actually present to facilitate the AP-sensor communication (for data querying, sensing control directives etc.), WiFED Mobile piggybacks energy level information in the VHT MIMO Control field of CBA that has two unused bits, as shown in Figure 7. These two bits represent the four discrete energy states of the sensor as shown in the Table I, with $1.8V$ and $3.6V$ being the minimum and maximum operational energy limits. Note that these fields are populated only if there is a change from the previous reported energy level, else the bits remain unused. Additionally, we emphasize that sensors themselves do not participate in data/communication beamforming with the AP.

On receiving the CBA frame, the AP forwards the bit level information to the controller along with the Authentication ID (AID) of the sensor. From the energy levels from Table I, sensors reporting '00' will have the highest priority for their energy request; those reporting '11' will have the least priority. The controller translates the bit level information to the lowest voltage value in the corresponding energy range and proceeds

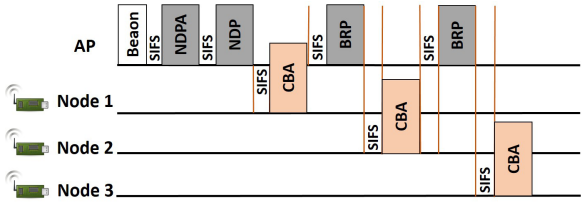

Fig. 8. WiFED Mobile sensor residual energy update through CBA frames during channel sounding procedure of 802.11ac protocol.

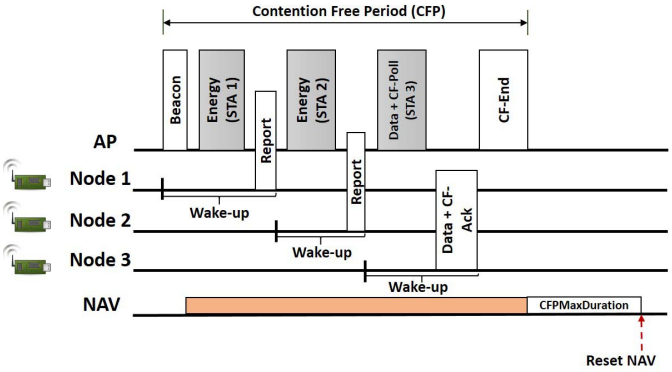

Fig. 9. WiFED Mobile scheduling of energy and data during 802.11ac contention free period.

to perform the energy monitoring, prediction, scheduling and sensor-ET mapping for beamforming, explained later in Section V.

C. Channel Reservation for Energy Transfer

The controller calculates the duration for the contention free period (CFP) based on the collective energy needs of the sensors, using the mathematical calculations in Sec. V. The AP then performs the following steps (see Figure 9):

- It activates Point Co-ordination Function (PCF) to create a CFP that will use a brief duration of TDMA for energy transfer. Thus, there are intermittent TDMA-based PCF sessions within an existing contention-based regular DCF time duration.
- The network allocation vector (NAV) for all clients and sensors is set by the AP to the maximum expected duration of the CFP (`CFPMaxDuration` parameter).
- All frame transfers during CFP use an inter-frame spacing that is less than that of DCF-based medium access, preventing other clients/sensors from gaining access to the medium using contention based mechanisms.
- At the end of the CFP, the AP resets the NAV of all stations (including sensors) and resumes regular contention based access.

- **Starting/ending Energy Transfer Durations:** The AP announces the CFP (and upcoming energy transfer) to the network using the beacon frame. The AP terminates the CFP by transmitting a CF-End frame, which resets the NAV of all the stations (including sensors) in the BSS [26]. For those sensors scheduled for energy transfer, the AP includes the sensor's AID in the beacon frame transmitted at the start of

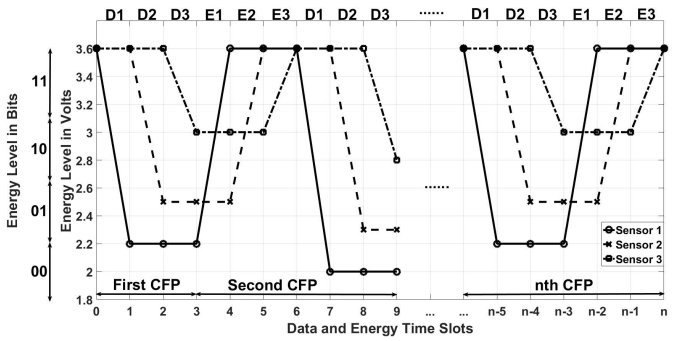

Fig. 10. Sensor residual energy graph during WiFED Mobile CFP operation of energy and data transfer.

CFP to inform the schedule of energy and data transfer slots for individual energy depleted sensors. Since the sensors wake up at the beacon intervals, they receive this information and accordingly wake up at their respective scheduled time slots for either energy or data transfer. We note that WiFED Mobile introduces delays in both PCF and DCF data traffic for STAs at the cost of supplying timely energy to the sensors. We provide quantitative results on this tradeoff later in Sec. VI.

• **Sensor Residual Energy Representation and Prediction:** In Figure 10, the residual energy representation of three sensors is depicted through data and energy time slots in CFP. The controller divides the CFP durations into fixed data and variable energy slots for each of the three sensors. The energy slots are variable, since the controller calculates the time to charge each sensor based on their differing residual energy at the start of every CFP. Sensor 1 data and energy slots are depicted as D1 and E1, respectively, and similarly D2, E2 for Sensor 2. The energy consumption is different as each sensor is assumed to have varied application data requirements. Sensor 1 consumes most energy followed by Sensor 2 and 3, in their respective data slots. With the current bit-level energy information received from the sensors, the controller also checks if each sensor's residual energy will go below the minimum threshold for sensor operation (1.8V). If the predicted residual energy is below the threshold for a sensor, it is added in the set of energy depleted sensors and controller schedules it for energy transfer in the next CFP. In Section V, we give detailed steps for the above calculations.

V. WiFED Mobile Energy Scheduling Framework

This section formally describes the mathematical operations performed by the controller to efficiently charge a large set of energy depleted sensors while minimizing the data communication delay. The first problem is how to identify the best subset of sensors for charging in the next CFP, without resulting in a fully energy depleted sensor. Furthermore, the formulation must also consider that other healthy sensors do not die out in the subsequent data slot, given their variable rates of data transfer for each data slot. Finally, the controller minimizes the overall charging rate for all the scheduled sensors with the limited number of ETs. The controller achieves these multiple objectives through an energy prediction scheme and global charging optimization, as described below.

A. Sensor Residual Energy Prediction

We assume the transmission power of the sensors for data transmission is fixed. Let, the sensor's transmission power for data transmission be $p^{eh}(t)$ and the start and end times for the data slot be t_{x-1} and t_x respectively. Then, energy consumed till the end of this data slot is $E_{C_{t_x}} = \int_{t_{x-1}}^{t_x} p^{eh}(t)$.

Let the transmission power of the sensor be fixed during energy charging, given as $p_f^{eh}(t)$. Then with t_{x-2} and t_{x-1} being the start and end times for energy harvesting, the energy consumed during energy harvesting at the end of this time slot can be given as

$$E_{Cf_{t_{x-1}}} = \int_{t_{x-2}}^{t_{x-1}} p_f^{eh}(t).$$

If V_{max} is the maximum voltage capacity of the sensor and t_{x-2} is the end of a data slot, at which instant, the residual energy is V_{res}. Then, the required energy status at t_{x-2} for the sensor is:

$$E_{req} = [C\frac{V_{max}^2 - V_{res}^2}{2}] \tag{2}$$

with C being the capacitor capacitance and the constraint $V_{res} \leq V_{max}$. Considering charging completes at t_{x-1}, the amount of energy that needs to be harvested in this sensor is:

$$E_{H_{t_{x-1}}} = E_{req} \tag{3}$$

with the constraint that the harvested energy $E_{H_{t_{x-1}}}$ should not exceed the maximum energy storage capacity E_{max} of the sensor:

$$E_{H_{t_{x-1}}} \leq E_{max} \tag{4}$$

Given the sensor being charged from t_{x-2} to t_{x-1} and is assigned a data slot from t_{x-1} to t_x, we formulate the residual energy at the end of time instant t_x as:

$$E_{res_{t_x}} = E_{res_{t_{x-1}}} - E_{C_{t_x}} \tag{5}$$

$$E_{res_{t_x}} = E_{H_{t_{x-1}}} - E_{Cf_{t_{x-1}}} - E_{C_{t_x}} \tag{6}$$

Substituting the values of $E_{H_{t_{x-1}}}$, $E_{Cf_{t_{x-1}}}$ and $E_{C_{t_x}}$ we get the following:

$$E_{res_{t_x}} = C\frac{V_{max}^2 - V_{res}^2}{2} - \int_{t_{x-2}}^{t_{x-1}} p_f^{eh}(t) - \int_{t_{x-1}}^{t_x} p^{eh}(t) \tag{7}$$

The controller decides to schedule the data transmission for a sensor in the next time slot based on: (i) the status of the residual energy at the end of the current time slot, (ii) prediction of residual energy after the next data slot in this case t_{x+1}.

$$E_{res_{t_{x+1}}} = E_{res_{t_x}} - E_{C_{t_{x+1}}} \tag{8}$$

$$E_{res_{t_{x+1}}} = [C\frac{V_{max}^2 - V_{res}^2}{2}]_{t_{x-1}} - \int_{t_{x-1}}^{t_x} p^{eh}(t) - \int_{t_x}^{t_{x+1}} p^{eh}(t) \tag{9}$$

The controller checks whether this residual energy at the next time slot after data transmission is higher than the

minimum threshold energy level required for all sensors, formulated as $C\frac{V_{min}^2}{2}$, where $V_{min} = 1.8\ Volts$ is the minimum voltage required by all sensors to remain alive. If the predicted residual energy in the next slot, due to data transmission, is greater than the minimum energy level, given as:

$$E_{res_{t_{x+1}}} > C\frac{V_{min}^2}{2}, \tag{10}$$

then the controller schedules a time slot from t_x to t_{x+1} for that sensor's data transmission. Otherwise, the controller schedules energy harvesting for that particular sensor at a future slot. The received power at the sensor due to energy beamforming is given by (1), which is exponential to the number of ETs. Thus, from (1) and (2), the time t to fully charge a sensor is calculated as:

$$P_T^r(t) = E_{req} \tag{11}$$

$$t_{charge} = \frac{C(V_{max}^2 - V_{res}^2)}{2P_T^r} \tag{12}$$

B. Optimization for Minimizing Charging Time

After calculating the amount of required energy and prediction of residual energy of each sensor, the controller performs the following optimization for minimizing charging time. We use K to N bipartite matching, where K ETs can be represented as a set of K nodes C_1, C_2, C_3.. C_i.. C_K [$1 \leq i \leq K$] and N sensors by a set of N sensors as v_1, v_2,.. v_j.. v_n [$1 \leq j \leq n$]. Given a deployment of K ETs and n sensors with energy requests, $(n < N)$, harvested power in the 802.11ac contention free time T [$1 \leq t \leq T$] at a sensor v_j can be calculated as:

$$E_j = \eta P_j^r(t) \tag{13}$$

where η is the RF-to-DC efficiency of the energy harvesting circuit, and $P_j^r(t)$ is the received power at sensor v_j (equation 1). Accordingly, the optimization problem is to maximize the overall harvested power of the n sensors within the contention-free time reserved earlier:

$$maximize \sum_{j=1}^{n} E_j \tag{14}$$

subject to the following constraints:

$$X_{ijt} \in 0,1 \quad [1 \leq i \leq K], [1 \leq j \leq n], [1 \leq t \leq T] \tag{15}$$

$$X_{ijt} = 0 \quad if \quad [t < 1] \quad and \quad [t > T] \tag{16}$$

$$\sum_{j=1}^{n} X_{ijt} \leq 1 \tag{17}$$

$$\sum_{i=1}^{K} X_{ijt} \leq K \tag{18}$$

where (15) states that $X_{ijt} = 1$, if ET C_i is charging sensor v_j in the designated time slot t, and otherwise $X_{ijt} = 0$. Also, (16) states the sensor v_j cannot be charged outside the contention-free time period T. Additionally, (17) states that ET C_i cannot charge more than one sensor v_j in the designated time slot t and (18) indicates that sensor v_j can be charged by more than one ET in the designated time slot t. (17) and (18) indicate one ET cannot charge more than one sensor at a time, while one sensor can be charged by more than one ET at a time. Thus, we define a set of virtual nodes for each sensor to enable concurrent ET assignment to the energy requesting node. In particular, each sensor has K virtual nodes that are designated to the available ETs. The weight of the edge connecting a virtual sensor node to one ET is represented by the harvested power contributed by the ET to the given sensor. The higher the harvested power, the weight of the link also increases, given the non-linear harvesting circuit efficiency [27]. We solve the mapping of K ETs to N nodes by using maximum weighted matching algorithm, as shown in Figure 11. The combined weights of the edges between ETs and virtual nodes of a sensor indicate the harvested power for that sensor, and the more ETs are assigned to a sensor, the higher its harvested voltage (and the lower its charging time) become.

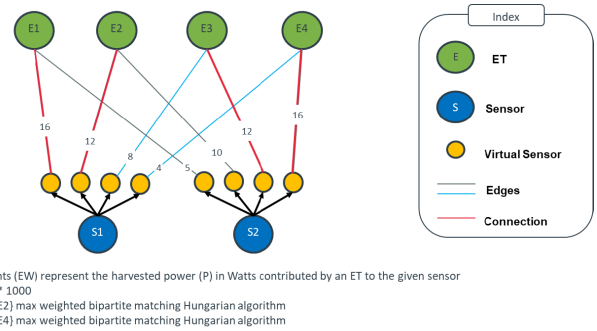

Fig. 11. Bipartite maximum weighted matching for scheduling ETs and sensors within each subgroup.

C. Scheduling ETs and Sensors

Our maximum weighted matching algorithm utilizes the Hungarian algorithm [28] to efficiently map the ETs with the energy depleted sensors in a given bipartite graph. We define disjoint sets $ET = \{ET_1, ET_2, \ldots, ET_K\}$ and $S = \{S_1, S_2, \ldots, S_N\}$ and form the bipartite graph, $G_{K,N}$, by taking ET and S as set of the bipartition of the vertex set of the graph. After the construction of the bipartite graph, optimal matching guarantees that each sensor gets one or more ET in a defined time slot. Algorithm 1, shows two main phases: (1) *initialization phase*, where we compute the weights based on the harvested power, and (2) *maximum weighted matching phase*.

At 802.11ac NDP duration, let N sensors demand energy from K ETs. The controller sorts the sensors in ascending order of their residual energy level. Then, it divides N sensors into n subgroups [n_1, n_2,.. n_i,.. n_n] such that the maximum number of sensors in each group is allocated as $\lceil K/2 \rceil - 1$ and total number of subgroups would be $\lceil \frac{N}{\lceil K/2 \rceil - 1} \rceil$. This guarantees each sensor will be assigned two and more ETs for distributed beamforming. Figure 11 depicts the corresponding constructed graph for each subgroup, where an edge represents all possible relations from a given sensor to ETs and the line

Algorithm 1 Scheduling ETs and Sensors

for $i \leftarrow 1$ to N **do**
  $E_{res_{t_{x+1}}} \leftarrow$ *compute* $\forall i \in N$
  if $E_{res_{t_{x+1}}} < C\frac{V_{min}^2}{2}$ **then**
    Schedule for energy harvesting
    for $j \leftarrow 1$ to K **do**
      $w_{i,j} \leftarrow P_{eh}(t)$
    end for
  end if
end for
Sort sensors according to E_{res} in ascending order
Create $n = \lceil \frac{N}{\lceil K/2 \rceil - 1} \rceil$ subgroups with max $\lceil K/2 \rceil - 1$ nodes per group
for $m \leftarrow 1$ to n **do**
  $i = (m-1) \times (\lceil K/2 \rceil - 1) + 1$
  $j = m \times (\lceil K/2 \rceil - 1)$
  Constitute KxK complete bipartite graph based on K ETs and virtual nodes associated from n_i to n_j
  Best Matching(m) $\leftarrow$ use Hungarian algorithm to get the maximum weighted matching
end for
return Best Matching

connection represents the assignments between ETs and sensor pairs based on their weights. The sensors in subsets [n_1, n_2,.. n_i,.. n_n] are in ascending order of residual energy level, i.e., the sensors in n_1 have the least residual energy while the sensors in n_n have the highest residual energy. Additionally, sensors are assigned charging time slots in ascending order of the residual energy. n_1 is assigned the first slot while n_n is assigned the last slot. The matching algorithm picks the best ETs to charge each sensor in the group n_i at the i_{th} time slot. After this selection, the duration of the i_{th} slot is calculated based on the maximum time to finish the simultaneous charging of all the sensors in the group n_i. Similar mapping and calculation for charging time is completed for the remaining n_{n-i} groups. In this way, the controller calculates the time duration for each slot and the overall required charging time for N sensors. The data slots for the 802.11ac users is allocated in the CFP time after charging the sensors.

D. Scheduling METs and Outlier Sensors

As mentioned before, there may be critical cases where the deployed sensors are located at the edge of deployment area or they may be located at far away distances from the installed static ETs, termed as outliers (OS). With the current algorithm setup, it can be inferred that since the installed ETs are located at large distances from the OS, the received power P_T^r, at each of these OS will be far less, resulting in over large charging time. This scheduling and optimization process with METs and OS, is termed as WiFED Mobile, which serve as an enhancement of WiFED beamforming with static ETs and in-range sensors. To identify the OS from the given set of sensors, a threshold for the received power is defined, given as $P_{T_{th}}^r$, the details of which are given below:

$$OS_j = 1 \quad if \quad [P_{T_j}^r < P_{T_{th}}^r] \quad for \quad all \quad [1 \leq i \leq K] \quad (19)$$

$$OS_j = 0 \quad if \quad [P_{T_j}^r > P_{T_{th}}^r] \quad for \quad all \quad [1 \leq i \leq K] \quad (20)$$

Equation (19) and (20) states that a given sensor OS_j, with $[1 \leq j \leq n]$, is an outlier (OS) if the received power at that sensor is less than the threshold received power from each and all available static ETs in the deployment area. Scheduling these OS for energy transfer through static ETs will result in creation of large CFPs, which will adversely affect both energy and data transfer efficiency of the entire system. This leads to defining an optimization problem that allocates METs with the aim of minimizing the charging time of OS, which is a subset of total n sensors, without degrading the energy transfer performance of the overall set of n sensors:

$$minimize \sum_{OS=1}^{m} t_{charge_{OS}} \quad (21)$$

where $[m < n]$ and METs and OS being subject to the same constraints as defined in Equations [15 - 18]. Additionally, there is also the constraint of:

$$\sum_{OS=1}^{m} X_{ijt} = 0 \quad (22)$$

which states that ET C_i cannot charge any OS v_j in the designated time slot t. Placing dedicated static ETs to serve individual OS is not cost-effective and scalable. Thus, a set of mobile ETs (METs) are deployed, which can dynamically place themselves closer to the OS, hence improving the P_t^r and reducing the energy transfer time, before moving on to the next OS. Similar, as in the case of allotment of static ETs to sensor nodes, described in Sec. V-B, the maximum weighted bipartite matching algorithm is applied here with a few modifications to take into account the mobility of the METs. Thus, we define a set of virtual nodes for each OS to enable concurrent MET assignment to the energy requesting OS. The weight of the edge connecting a virtual OS node to one MET is represented by the distance of the MET to the given OS, for a particular time slot t, as $D_{eh}(t)$. The smaller the distance, the higher is the weight of the link, given the proportionality between distance and received power and the non-linear harvesting circuit efficiency [27]. We solve the mapping of K METs to N OS nodes by using maximum weighted matching algorithm, as shown in Figure 11. The combined weights of the edges between METs and virtual OS nodes indicate the harvested power for that OS, and the more METs are assigned to a OS, the higher its harvested voltage (and the lower its charging time) become. In this scheduling algorithm, we define disjoint sets $MET = \{MET_1, MET_2, \ldots, MET_K\}$ and $OS = \{OS_1, OS_2, \ldots.., OS_M\}$ and form the bipartite graph, $H_{K,N}$, by taking MET and OS as set of the bipartition of the vertex set of the graph.

At 802.11ac NDP duration, let M OS demand energy from K METs. The controller sorts the OS in ascending order of their residual energy level. Then, it divides M sensors into m subgroups [m_1, m_2,.. m_i,..,m_m] such that the maximum

Algorithm 2 Allocating METs to OS

Keep count of energy transfer instance
for $p \leftarrow 1$ to K **do**
  if $location_p$ has changed after last iteration of energy transfer and Energy transfer instance > 0 **then**
    $counter_p = 1$
  else
    $counter_p = 0$
  end if
end for
for $i \leftarrow 1$ to M **do**
  $E_{res_{t_{x+1}}} \leftarrow$ *compute* $\forall i \in M$
  if $E_{res_{t_{x+1}}} < C\frac{V_{min}^2}{2}$ **then**
    Schedule for energy harvesting
    for $j \leftarrow 1$ to K **do**
      if $counter_j = 1$ and OS_i was not in last energy transfer instance **then**
        $w_{i,j} \leftarrow D_{eh}(t)$
      end if
    end for
  end if
end for
Sort sensors according to E_{res} in ascending order
Create $m = \lceil \frac{M}{\lceil K/2 \rceil - 1} \rceil$ subgroups with max $\lceil K/2 \rceil - 1$ nodes per group
for $o \leftarrow 1$ to m **do**
  $i = (o-1) \times (\lceil K/2 \rceil - 1) + 1$
  $j = o \times (\lceil K/2 \rceil - 1)$
  Constitute KxK complete bipartite graph based on K METs and virtual nodes associated from m_i to m_j
  Best Matching(m) $\leftarrow$ use Hungarian algorithm to get the maximum weighted matching
end for
return Best Matching
Energy transfer instance + 1

number of OS in each group is allocated as $\lceil K/2 \rceil - 1$ and total number of subgroups would be $\lceil \frac{M}{\lceil K/2 \rceil - 1} \rceil$. This guarantees each sensor will be assigned two or more METs for distributed beamforming. Similar to Figure 11, the generated graph depicts the corresponding constructed graph for each subgroup. Here, an edge represents all possible relations from a given OS to METs and the line connection represents the assignments between METs and OS pairs based on their weights. The preference of pairing is given on how near the MET is from a given OS. Here, if the MET has not changed location from the previous instance of energy transfer, then the controller skips the redundant step of calculating the link weights for those METs paired with OS, which were also in the previous energy transfer instance. After MET allocation, the assigned METs are made to move as near to the OS as possible. The maximum traverse time t_{tr}^j, for a MET j with $[1 \leq j \leq K]$, among this subset of assigned METs, is then taken as the total available CFP time, $CFP_{potential}$, for BF with static ETs to normal sensors, given by,

$$t_{tr}^j = CFP_{potential} \tag{23}$$

The AP chooses to assign static ETs to BF to other sensors, according to the energy demand, during the $CFP_{potential}$ time or may choose to run DCF for the duration of $CFP_{potential}$ and then revert back to PCF for BF with METs to OS. The OS in subsets [m_1, m_2,.. m_i,.. m_m] are arranged in ascending order of residual energy level, and the charging time slots are assigned in ascending order of residual energy also. After this the controller assigns charging slots for each OS and calculates the CFP duration in similar fashion as with static ETs to sensors energy transfer, described in Sec. V-C.

VI. Performance Evaluation

In this section, we extensively evaluate data and energy performance metrics of the WiFED. We have implemented our system through integration of a distributed energy transfer module with NS-3. First, we evaluate system wireless energy transfer performance without OS in terms of charging time. Then, we investigate the system data performance in terms of packet error rate, average throughput, and latency by comparing with three schemes: 802.11ac with random energy transmission, 802.11ac with continuous data transmission, and 802.11ac without energy transfer. After this, we extend the evaluation by introducing OSs in the system and comparing the performance of WiFED and WiFED Mobile in terms of throughput and latency.

A. Simulation Setup

We consider variable number of sensors that are randomly deployed in 20×20 m^2 area with multiple mobile and static ETs and in a space with an active 802.11ac AP connected to a controller. We run the simulation 300 times at each instance of number of sensors, ETs, packet size and packet numbers. Before each evaluation, the batteries on each sensor are set to a maximum voltage level, $V_{max} = 3.65$ Volts. The characteristics of the sensor, such as power of transmission, reception, sensing, sleeping, channel bandwidth are set based on micro-controller TI MSP430F2274, and 2.4 GHz CC2500 radio chip. The capacitance of the capacitor, C, is 5700μF, and all ETs have the same transmission power as $P_t = 3$ Watts. Transmitter and receiver antenna gain are set to $G_t = 3.98$ dBi, and $G_r = 1$ dBi. Movement speed of mobile ET is $2m/s$ and the $P_{T_{th}}^r$ is set at 0.01 W.

B. Energy and Data Performance Analysis of WiFED

As the baseline energy performance comparison, Figure 12(a) shows a distance-based matching scenario where the controller groups the sensors according to the position of ETs. Figure 12 presents the WiFED scenario where the sensors are scheduled into optimal subgroups (SGs) via our bipartite matching algorithm from Sec. V-C. First, we set the number of ETs at 10 and the number of sensors at 40, and measure the required energy level of each sensor according to residual energy level with equation (2), shown

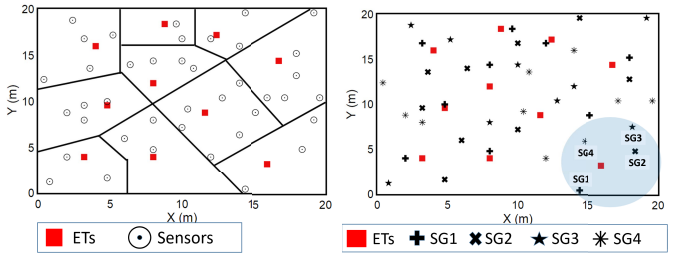

(a) (b)

Fig. 12. Two scenarios of network topology: N=40, K=10 (a) Closest distance assignment (b) WiFED assignment into subgroups based on residual energy.

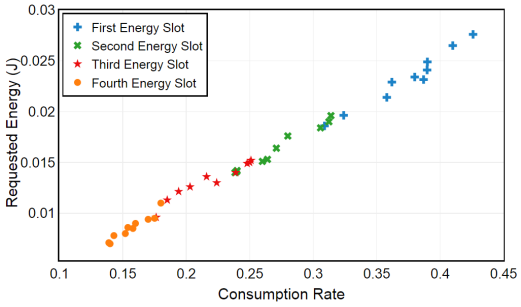

Fig. 13. Requested energy level (J) w.r.t. consumption rate for 40 sensors at a time interval.

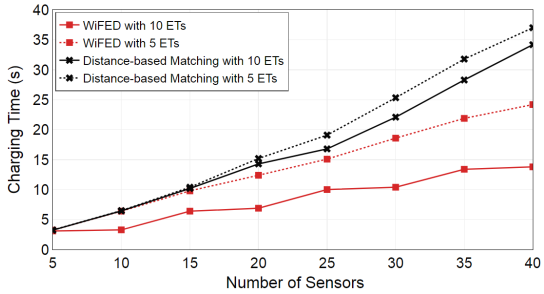

Fig. 14. Charging time (s) w.r.t number of sensors.

in Figure 13. We calculate the ratio of consumed energy at a given time instant and accordingly show the scheduling of sensors to be served in subsequent energy slots. We see that almost all the nodes with high energy consumption rates are scheduled for energy harvesting in the first slot. Additionally, residual energy and consumption rates are not unique and independently impact the energy harvesting in a time slot.

Figure 14 shows the average charging time with deployment of 5 and 10 ETs. We see that WiFED provides significant improvement in terms of charging time compared to the distance based scenario. Synchronizing transmit and receive times at sensors and scheduling the ETs over sensors have enabled 15% improvement in network lifetime due to less time to charge. In distance-based matching scenario, we observe that when sensors are deployed in higher density, more sensors die out as each ET can only serve a limited number of sensors within its range. This method is also unable to predict the priority of sensors and each ET randomly transfers power to

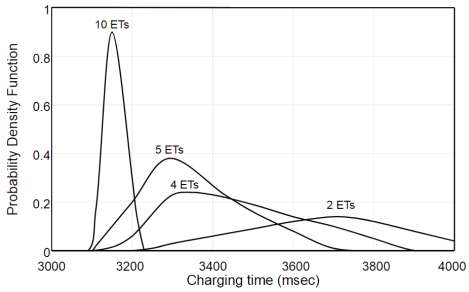

Fig. 15. Probability density function of charging time (msec) for one node. The number of ETs is defined as 10, 5, 4 and 2. The number of sensors is equal to 5.

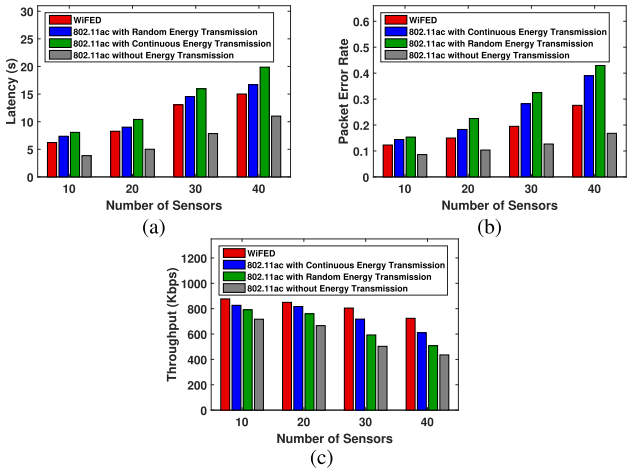

Fig. 16. (a) Latency (b) Packet error rate (c) Throughput w.r.t. varying number of sensor.

the sensors within its operation area. A node that is far away from the ET will have a lower energy harvesting level than a closer one to the ET. In this case, energy levels of sensors are not taken into account and there is no mechanism to gather information such as requested energy, residual energy, and consumed energy.

We next investigate how charging time changes based on the number of ETs. Figure 15 shows the probability density function of charging time for one sensor. Here, we set the number of sensors to 5. As seen in the Figure 15, when the number of ETs increases to 10, the probability of each sensor getting charged by more than one ET at a time will increase and this will result in a lower charging delay. On the other hand, when the number of sensors is higher than the number of ETs, such as 2 ETs, the controller groups the sensors based on the residual energy and data transmission, and then schedules the sensors. Compared to distance-based matching, WiFED contributes 31% reduction in the charging delay.

For calculating the data performance, we simulate four scenarios with varying number of sensors and ETs: (i) WiFED, (ii) 802.11ac with Random Energy Transmission (RET), (iii) 802.11ac with Continuous Energy Transmission (CET), and (iv) 802.11ac without energy transmission. We compare the results as seen in Figure 16 in terms of latency, packet error rate and throughput.

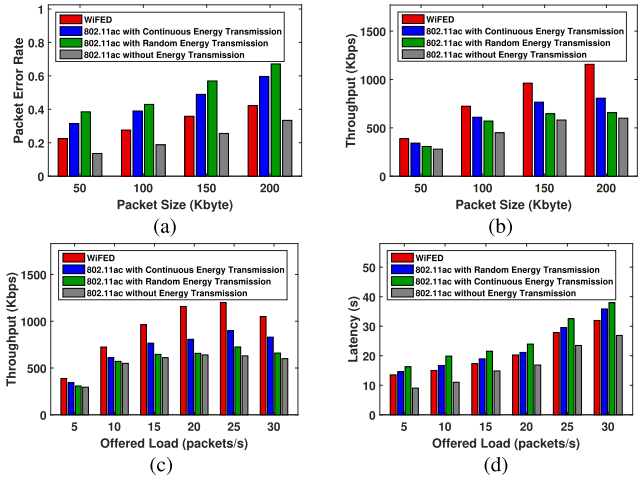

Fig. 17. (a) Packet error rate and (b) Throughput w.r.t. packet size when offered load is equal to 10 packets/s (c) Throughput and (d) Latency w.r.t. offered load (packet/s) when packet size is equal to 100Kbytes.

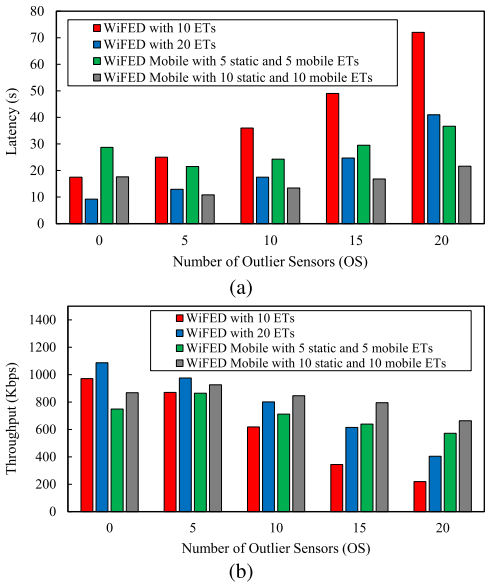

Fig. 18. (a) Latency and (b) throughput w.r.t. number of outlier sensors.

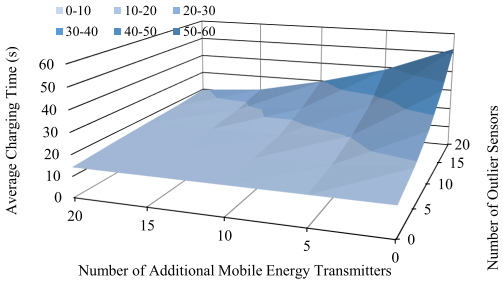

Fig. 19. Average charging time of WiFED with Mobile ETs.

To measure latency, the packet generation rate is set to 10 packets per second, with packet size of 100KB. As shown in Figure 16(a), WiFED experiences much less latency, compared to 802.11ac with RET and CET, because WiFED manages the energy transfer process to co-exist with WiFi. We calculate PER and throughput in the four scenarios given in Figures 16(b)-16(c). To measure PER, the number of packets correctly received are observed along with their respective signal strengths. The average throughput per node is calculated for varying number of sensors. We observe a significant improvement in WiFED throughput and PER, due to the co-existence support. On the other hand, with 802.11ac RET and CET, the probability of data signals being interrupted greatly increases, resulting in higher packet error rate and reduced throughput. Interestingly, Figure 16(c) shows the throughput of the network is better in WiFED than in the scenario with no energy transfer. Also, RET and CET scenarios perform better than in the case of no energy transfer. This is because in RET and CET, because of no scheduling, some sensors get completely depleted of energy and stop transmitting data, whereas those sensors in the region of energy reception cannot transmit data because of interference. This creates *holes* in the network topology that decreases the number of competing users for channel access. Also, the WiFED controller co-ordinates data and energy transfer in a time scheduled manner, which negates the eliminates such *holes* and interfering signals. From Figure 17, we see the results of data transmission in our four scenarios with varying number of packet size and offered load (packets/s). We conduct the simulation with 10 ETs and 40 sensors. These results show that both 802.11ac RET and CET adversely affects the performance of data and energy transmission. Thus, WiFED provides better results in terms of throughput and packet error rate while 802.11ac with RET and CET offers no improvement in data transmission.

C. Performance Analysis of WiFED Mobile

In this part of the simulation, we first investigate how OSs in the system nullifies the overall performance improvement of WiFED by drastically increasing the average charging time. Then, we show how WiFED Mobile mitigates this deficiency by incorporating METs.

Figure 18 shows latency and throughput results with and without METs for varying number of OS where overall number of sensors is always equal to 40. As seen in both figures, WiFED (without any MET) performs better in the scenario where there are no OS in the system when compared to its counterpart with same number of transmitters, including METs. For the sake of simplicity, we assume that WiFED Mobile controller will utilize METs only to serve OSs. Thus we have METs instead of static ETs in the scenarios where there are few to none OS, which would otherwise, increase the overall time required to charge sensor, leading to less throughput with high latency. On the other hand, WiFED with only static ETs suffers greatly when number of OS is increasing since limited power reception at OS will greatly increase the interval used to transfer energy in CFPs. This situation creates two-fold negative impact on throughput and latency, (1) it diminishes the time intervals that otherwise could be used for data transmission and (2) high charging times causes some sensors to get depleted completely and impairs the overall throughput.

In the second part of this evaluation, we investigate the average charging time for the scenarios where there are overall

40 sensors that consists of varying number of OSs and 10 static ETs with the additional number of METs that varies between 0 and 20. Figure 19 shows the strict relation between METs and OS. As seen in this figure, when there are high number of OSs and insufficient number of METs to supply necessary charging, average charging time increases exponentially. On the other hand, average charging time converges to its optimal value, when there is an over-provision of METs in the system.

VII. Conclusion

We devised a data and energy co-existence approach using in-band 802.11ac protocol defined features for distributed energy beamforming through dedicated transmitters. We demonstrated the feasibility of a practical system with preliminary experiments and extensive simulations. We also showcased the unfavorable effects of outlier sensors and proved that they are easily mitigated with the efficient incorporation of mobile energy transmitters into the architecture. Comparing the performance of data and energy delivery in WiFED with constant and random energy transfers, we see that our approach enables seamless co-existence within the legacy WiFi protocols, while achieving 31% reduction in charging delay and 15% improvement in sensor lifetime. Further investigations also showed that utilizing mobile energy transmitters provide reduction in latency up to 42% and improves throughput up to 83 % in the scenarios where static ETs fail to satisfy charging cycles of outlier sensors.

References

[1] X. Lu, P. Wang, D. Niyato, D. I. Kim, and Z. Han, "Wireless charging technologies: Fundamentals, standards, and network applications," *IEEE Commun. Surveys Tuts.*, vol. 18, no. 2, pp. 1413–1452, 2nd Quart., 2016.

[2] T. Banerjee, K. R. Chowdhury, and D. P. Agrawal, "Using polynomial regression for data representation in wireless sensor networks," *Int. J. Commun. Syst.*, vol. 20, no. 7, pp. 829–856, 2007.

[3] O. L. A. López, H. Alves, R. D. Souza, S. Montejo-Sánchez, E. M. G. Fernández, and M. Latva-Aho, "Massive wireless energy transfer: Enabling sustainable IoT towards 6G era," 2019, *arXiv:1912.05322*. [Online]. Available: http://arxiv.org/abs/1912.05322

[4] Y. Zeng, B. Clerckx, and R. Zhang, "Communications and signals design for wireless power transmission," *IEEE Trans. Commun.*, vol. 65, no. 5, pp. 2264–2290, May 2017.

[5] R. Mudumbai, J. Hespanha, U. Madhow, and G. Barriac, "Distributed transmit beamforming using feedback control," *IEEE Trans. Inf. Theory*, vol. 56, no. 1, pp. 411–426, Jan. 2010.

[6] F. Quitin, M. M. U. Rahman, R. Mudumbai, and U. Madhow, "Distributed beamforming with software-defined radios: Frequency synchronization and digital feedback," in *Proc. IEEE Global Commun. Conf. (GLOBECOM)*, Dec. 2012, pp. 4787–4792.

[7] S. Mohanti, E. Bozkaya, M. Yousof Naderi, B. Canberk, and K. Chowdhury, "WiFED: WiFi friendly energy delivery with distributed beamforming," in *Proc. IEEE Conf. Comput. Commun. (INFOCOM)*, Apr. 2018, pp. 926–934.

[8] FCC. *FCC Rules*. Accessed: Sep. 21, 2019. [Online]. Available: https://www.fcc.gov/general/rules-regulations-title-47

[9] N. S. P. Nandiraju, H. Gossain, D. Cavalcanti, K. R. Chowdhury, and D. P. Agrawal, "Achieving fairness in wireless LANs by enhanced IEEE 802.11 DCF," in *Proc. IEEE Int. Conf. Wireless Mobile Comput., Netw. Commun. (WiMob)*, Jun. 2006, pp. 132–139.

[10] Z. A. Eu, H.-P. Tan, and W. K. G. Seah, "Design and performance analysis of MAC schemes for wireless sensor networks powered by ambient energy harvesting," *Ad Hoc Netw.*, vol. 9, no. 3, pp. 300–323, May 2011.

[11] X. Fafoutis and N. Dragoni, "ODMAC: An on-demand MAC protocol for energy harvesting–wireless sensor networks," in *Proc. 8th ACM Symp. Perform. Eval. Wireless Ad Hoc, Sensor, Ubiquitous Netw. (PE-WASUN)*, 2011, pp. 49–56.

[12] R. G. Cid-Fuentes, M. Y. Naderi, S. Basagni, K. R. Chowdhury, A. Cabellos-Aparicio, and E. Alarcon, "On signaling power: Communications over wireless energy," in *Proc. 35th Annu. IEEE Int. Conf. Comput. Commun. (INFOCOM)*, Apr. 2016, pp. 1–9.

[13] X. Lu, P. Wang, D. Niyato, D. I. Kim, and Z. Han, "Wireless networks with RF energy harvesting: A contemporary survey," *IEEE Commun. Surveys Tuts.*, vol. 17, no. 2, pp. 757–789, 2nd Quart., 2015.

[14] S. Lee, R. Zhang, and K. Huang, "Opportunistic wireless energy harvesting in cognitive radio networks," *IEEE Trans. Wireless Commun.*, vol. 12, no. 9, pp. 4788–4799, Sep. 2013.

[15] A. A. Nasir, X. Zhou, S. Durrani, and R. A. Kennedy, "Relaying protocols for wireless energy harvesting and information processing," *IEEE Trans. Wireless Commun.*, vol. 12, no. 7, pp. 3622–3636, Jul. 2013.

[16] X. Fan *et al.*, "Energy-ball: Wireless power transfer for batteryless Internet of Things through distributed beamforming," *Proc. ACM Interact., Mobile, Wearable Ubiquitous Technol.*, vol. 2, no. 2, pp. 1–22, Jul. 2018.

[17] O. Georgiou, K. Mimis, D. Halls, W. H. Thompson, and D. Gibbins, "How many Wi-Fi APs does it take to light a lightbulb?" *IEEE Access*, vol. 4, pp. 3732–3746, 2016.

[18] O. L. A. Lopez, H. Alves, R. D. Souza, and S. Montejo-Sanchez, "Statistical analysis of multiple antenna strategies for wireless energy transfer," *IEEE Trans. Commun.*, vol. 67, no. 10, pp. 7245–7262, Oct. 2019.

[19] W. Xu, W. Liang, S. Hu, X. Lin, and J. Peng, "Charging your smartphones on public commuters via wireless energy transfer," in *Proc. IEEE 34th Int. Perform. Comput. Commun. Conf. (IPCCC)*, Dec. 2015, pp. 1–8.

[20] M. Y. Naderi, K. R. Chowdhury, and S. Basagni, "Wireless sensor networks with RF energy harvesting: Energy models and analysis," in *Proc. IEEE Wireless Commun. Netw. Conf. (WCNC)*, Mar. 2015, pp. 1494–1499.

[21] Mathworks. *Multi-User Transmit Beamforming With USRP Hardware*. Accessed: Sep. 21, 2019. [Online]. Available: https://www.mathworks.com/help/supportpkg/usrpradio/examples/multi-user-transmit-beamforming-with-usrp-r-hardware.html

[22] R. Mudumbai, J. Hespanha, U. Madhow, and G. Barriac, "Scalable feedback control for distributed beamforming in sensor networks," in *Proc. Int. Symp. Inf. Theory (ISIT)*, 2005, pp. 137–141.

[23] R. Palacios-Trujillo, J. Alonso-Zarate, N. L. S. da Fonseca, and F. Granelli, "Maximum achievable energy efficiency of TXOP power save mode in IEEE 802.11ac WLANs," in *Proc. IEEE Global Commun. Conf. (GLOBECOM)*, Dec. 2016, pp. 1–7.

[24] G. Matthew, *802.11ac: A Survival Guide: Wi-Fi at Gigabit and Beyond*. Sebastopol, CA, USA: O'Reilly Media, 2013.

[25] *Wireless LAN Medium Access Control (MAC) and Physical Layer (PHY) Specifications–Amendment 4: Enhancements for Very High Throughput for Operation in Bands Below 6 GHz*, IEEE Standard 802.11ac-2013, Dec. 2013, pp. 1–425.

[26] E. Perahia and R. Stacey, *Next Generation Wireless LANs: 802.11n and 802.11ac*. Cambridge, U.K.: Cambridge Univ. Press, 2013.

[27] B. Canberk and S. Oktug, "A dynamic and weighted spectrum decision mechanism based on SNR tracking in CRAHNs," *Ad Hoc Netw.*, vol. 10, no. 5, pp. 752–759, Jul. 2012.

[28] H. W. Kuhn, "The Hungarian method for the assignment problem," *Nav. Res. Logistics Quart.*, vol. 2, pp. 83–97, Mar. 1955.

Subhramoy Mohanti (Graduate Student Member, IEEE) is currently pursuing the Ph.D. degree with the Department of Electrical and Computer Engineering, Northeastern University. His current research interests include aerial distributed beamforming, machine learning enabled UAV identification, UAV networking, wireless protocols and networks, scheduling, and optimization. He has published and coauthored many articles on these topics. He has served as a reviewer for numerous articles on these areas. He was a recipient of the IEEE INFOCOM Best Paper Award in 2018, the Northeastern University Graduate Dissertation Research Grant in 2015, for his Master's thesis, and NSF Travel Grant for IEEE INFOCOM 2018.

Elif Bozkaya (Graduate Student Member, IEEE) received the M.Sc. and Ph.D. degrees in computer engineering from Istanbul Technical University, Turkey, in 2015 and 2020, respectively. She was a Visiting Researcher with the Faculty of Computer Science, University of Vienna, Austria, from February 2019 to August 2019. She is currently a Teaching Staff with the Department of Computer Engineering, National Defense Naval Academy, Turkey. Her research interests include aerial networks, software-defined networking (SDN), vehicular networks, and sensor networks. She was a recipient of IEEE INFOCOM Best Paper Award in 2018.

M. Yousof Naderi (Member, IEEE) received the Ph.D. degree in electrical and computer engineering from Northeastern University, Boston, MA, USA, in 2015. He is currently a Research Assistant Professor with the Electrical and Computer Engineering Department, Northeastern University. His research interests include the design and development of software-defined wireless systems, wireless energy transfer and harvesting, and AI-enabled embedded solutions for next-generation cyber-physical systems. In these areas, he has coauthored numerous scientific journal and conference paper publications, served as a reviewer for more than 100 articles in journals and conferences, and a TPC and an organizer of several academic conferences and workshops. He was a recipient of NEU Ph.D. Dissertation Award in 2015, a Finalist in the Bell Labs Prize competition in 2017, and best paper awards at the IEEE INFOCOM in 2018 and IEEE GLOBECOM in 2019.

Berk Canberk (Senior Member, IEEE) has been an Adjunct Associate Professor with the Department of Electrical and Computer Engineering, Northeastern University, since 2016. He is currently an Associate Professor with the Department of Computer Engineering, ITU. He also serves as an Editor for IEEE COMMUNICATIONS LETTER, IEEE TRANSACTIONS IN VEHICULAR TECHNOLOGY, *Computer Networks* (Elsevier), and *Computer Communications* (Elsevier). His current research interests include software-defined networking (SDN), intelligent aerial networks, and next generation network management systems. He was a recipient of the IEEE Turkey Research Incentive Award in 2018, the IEEE INFOCOM Best Paper Award in 2018, The British Council (U.K.) Researcher Link Award in 2017, the IEEE CAMAD Best Paper Award in 2016, Royal Academy of Engineering (U.K.) NEWTON Research Collaboration Award in 2015, the IEEE INFOCOM Best Poster Paper Award in 2015, the ITU Successful Faculty Member Award in 2015, and the Turkish Telecom Collaborative Research Award in 2013.

Gokhan Secinti (Member, IEEE) was a Post-Doctoral Research Associate with Northeastern University from 2017 to 2019. He has been an Assistant Professor with Istanbul Technical University since 2019. His current research interests include software-defined networking and performance analysis of 5G networks. He currently serves as a reviewer for *IEEE Communications Magazine*, IEEE TRANSACTIONS ON VEHICULAR TECHNOLOGY, IEEE TRANSACTIONS IN WIRELESS COMMUNICATIONS, and *The International Journal of Communication Systems*. He was a recipient of the IEEE INFOCOM Best Poster Paper Award in 2015 and the IEEE CAMAD Best Paper Award in 2016.

Kaushik R. Chowdhury (Senior Member, IEEE) received the M.S. degree from the University of Cincinnati in 2006, and the Ph.D. degree from the Georgia Institute of Technology in 2009. He was an Assistant Professor from 2009 to 2015 and an Associate Professor from 2015 to 2020 with Northeastern University, where he is currently a Professor with the Electrical and Computer Engineering Department. His current research interests include dynamic spectrum access, wireless RF energy harvesting and IoT, and in the area of intra/on-body communication. He was a winner of the Presidential Early Career Award for Scientists and Engineers (PECASE) in 2017, the ONR Director of Research Early Career Award in 2016, and the NSF CAREER Award in 2015.